Bulletin de la Société Royale des Sciences de Liège, Vol. 84, 2015, p 53 - 59

Thermal processing of astrophysical ice analogs using the Interstellar Astrochemistry Chamber

Rafael Martín Doménech[1*], Guillermo M. Muñoz Caro[1]

[1] Centro de Astrobiología (INTA-CSIC), Ctra. de Ajalvir, km 4,
Torrejón de Ardoz, 28850 Madrid, Spain

Abstract: Thermal processing of astrophysical ices takes place in circumstellar environments. Knowledge of this process comes from a combination of astronomical observations and laboratory simulations under astrophysically relevant conditions. For the first time we present the results of temperature programmed desorption (TPD) experiments with realistic pre-cometary ice analogs composed of up to five molecular components: H_2O, CO, CO_2, CH_3OH, and NH_3. The experiments were performed with an ultra-high vacuum chamber. Volatiles desorbing to the gas phase were monitored using a quadrupole mass spectrometer, while changes in the ice structure and composition were studied by means of infrared spectroscopy. The TPD curves of water ice containing CO, CO_2, CH_3OH, and NH_3 present desorption peaks at temperatures near those observed in pure ice experiments, volcano desorption peaks after water ice crystallization, and co-desorption peaks with water. Desorption peaks of CH_3OH and NH_3 at temperatures similar to the pure ices takes place when their abundance relative to water is above $\sim$ 3 % in the ice matrix. We found that CO, CO_2, and NH_3 also present co-desorption peaks with CH_3OH, which is the only species that segregated enough to allow detection in the IR spectra. These results reproduce the heating of circumstellar ices in hot cores and can be also applied to the late thermal evolution of comets.

1 Introduction

Dense molecular clouds have typical densities of 10^4-10^6 particles cm^{-3} and temperatures down to 10 K in their interiors. Under these conditions, molecules are able to condense onto the surface of dust grains, forming ice mantles (see, e.g., Allamandola et al 1999, and ref. therein).

When a dense core collapses to form a star, grain agglomeration can take place during the cold core phase, leading to cluster particles composed of sub-micron grains. Later on, during the warm-up phase, the protostar heats its environment, leading to thermal processing of ice mantles. This thermal annealing takes place in two different ways. On the one hand, grains at a certain distance are heated (approximately 1 K/century; Viti & Williams 1999) as the temperature of the protostar increases. On the other hand, grains are also able to undergo periodic radial excursions to distances less than 0.1 AU from the central protostar on short timescales (from a few to hundreds of hours), according to the fluctuating X-wind model for the formation of Ca-Al-rich inclusions (CAIs) and chondrules (Shu et al. 1996, 1997, 2001). The main effect of thermal processing is the sublimation of ice mantles explaining

*rmartin@cab.inta-csic.es

the excess gas-phase abundances of some species in the inner regions of protostellar envelopes (e.g., Pauls et al. 1983; Herbst & van Dischoeck 2009 and ref. therein).

The remaining ice mantles in protoplanetary disks are incorporated in comets and other minor bodies. Cometary ice composition is thought to be similar to that of the interstellar ice mantles (Mumma & Charnley 2011 and ref. therein), although it can vary between comets. Cometary ices are also exposed to thermal processing, which is the main responsible for the activity observed in comets.

Most of our current knowledge on interstellar, circumstellar, and cometary ices comes from a combination of infrared observations and laboratory experiments that simulate their energetic processing under astrophysically relevant conditions. Heating of ice mixtures leads to structural changes in the ice, involving diffusion of molecules, phase changes, and ice segregation. Segregation is expected to occur whenever ice diffusion of molecules is possible, and it is energetically favorable for molecules of the same kind to group together. Ice diffusion barriers are proportional to the binding energy of the species (i.e., their volatility). Thermal annealing of ice samples also leads to sequential desorption of ice molecules, which starts with the most volatile species (Öberg et al. 2009).

This work represents the first attempt to study the thermal processing of realistic astrophysical ice analogs with up to five molecular components (H_2O, CO, CO_2, CH_3OH, and NH_3) using both mass spectrometry and infrared spectroscopy.

The layout of this paper is as follows. In Sect. 2, we describe the experimental protocol. Section 3 presents the experimental results. Their astrophysical implications are discussed in Sect. 4.

2 Experimental

The Interstellar Astrochemistry Chamber (ISAC) is an ultra-high vacuum (UHV) chamber with a pressure about 4 x 10^{-11} mbar, which corresponds to a density of 10^6 cm^{-3} (Muñoz Caro et al. 2010), similar to that found in dense cloud interiors. Ice samples made by deposition of a gas mixture onto a KBr window at 8 K (achieved by means of a closed-cycle helium cyostat) were warmed up with a controlled heating rate of 1-2 K/min until a complete sublimation was attained. Complex gas mixtures were prepared in the gas line system with the desired composition.

The chemical components used in the experiments were H_2O (liquid), triply distilled, CH_3OH (liquid, Panreac 99.9%), CO (gas, Praxair 99.998%), CO_2 (gas, Praxair 99.996%), and NH_3 (gas, Praxair 99.999%), which was deposited through a second deposition tube.

The evolution of the solid sample was monitored by in situ Fourier transform infrared (FTIR) transmittance spectroscopy, using a Bruker Vertex 70 spectrometer equipped with a deuterated triglycine sulfate detector (DTGS) , with a spectral resolution of 2 cm^{-1}. Column densities of each species in the ice were calculated from the IR spectra using the formula

$$N = \frac{1}{A} \int_{band} \tau_\nu \, d\nu, \tag{1}$$

where N is the column density in molecules cm^{-2}, τ_ν the optical depth of the absorption band, and A the band strength in cm molecule^{-1}, as derived from laboratory experiments.

The desorbing molecules were detected by a Pfeiffer Prisma QMS which is situated $\sim$ 17 cm apart from the sample.

All ice analogs had column densities above one hundred monolayers (1 ML is commonly defined as 10^{15} molecules/cm^2), which are well above the canonical thickness of a thin interstellar ice mantle ($\sim$ 40 ML; Bisschop et al. 2006). Therefore, these experiments more faithfully reproduce the thermal annealing of thicker ice mantles formed in cold circumstellar regions by grain agglomeration, and cometary ices (see Sect. 4). In addition, thick ice analogs prevent the substrate (KBr in this case) to have an influence on the desorption process of the molecules.

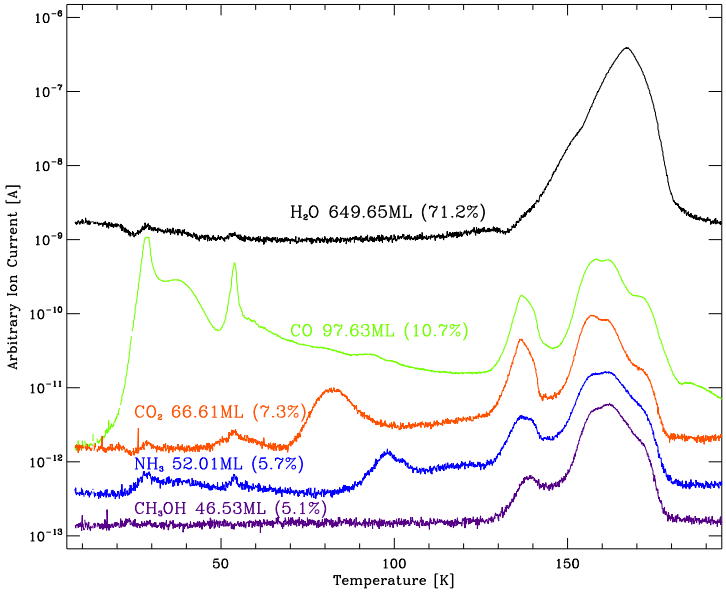

Figure 1: TPD curves of each component in a pre-cometary ice mixture. Heating rate was 2 K/min.

3 Results

3.1 Temperature programmed desorption curves

Figure 1 shows the temperature programmed desorption (TPD) curve of each ice component in a pre-cometary ice mixture co-deposited at 8 K and warmed up with a heating rate of 1 K/min. All species show desorption peaks at temperatures near the ones corresponding to pure ices. Desorption of NH_3 and CH_3OH at temperatures compatible with pure desorption was not previously documented for co-deposited mixtures (Collings et al. 2004; Brown et al. 2006). In our experiments, this kind of desorption took place when their abundance relative to water is above $\sim$ 3 % in the ice matrix (Martín-Doménech et al. 2014). Desorption of molecules from a pure ice environment is considered evidence of segregation occuring in the ice mixture, at least to some extent (Bisschop et al. 2006).

All the species except H_2O present desorption peaks at temperatures higher than the corresponding temperature for pure ices. This indicates that these molecules are retained in the water ice structure (Bar-Nun et al. 1985; Collings et al. 2004; Fayolle et al. 2011). A fraction of the trapped molecules is released in the "volcano" desorption (Smith et al. 1997) when the change from amorphous to cubic crystalline water ice occurs at T $\sim$ 160 K. Another fraction of the trapped molecules co-desorbs later with water, which peaks at T $\sim$ 171 K.

The three types of desorption described so far (desorption as for the pure ice, volcano desorption and co-desorption with water) are common to most of the binary mixtures with H_2O. However, co-desorption of the three most volatile species (CO, CO_2, and NH_3) with CH_3OH at T $\sim$ 146 K is also observed in the studied multicomponent mixtures in which desorption of methanol at a temperature near the one corresponding to the pure ice is detected (Martín-Doménech et al. 2014). These co-desorption peaks cannot be reproduced in binary ice mixtures with water.

3.2 Evolution of IR spectra during thermal processing

The IR spectrum of an ice analog mixture at 8 K is generally well reproduced by the sum of individual pure ice spectra (Fig 2). The observed differences are due to interactions between water molecules

and the rest of the components (Martín Doménech et al. 2014 and references therein).

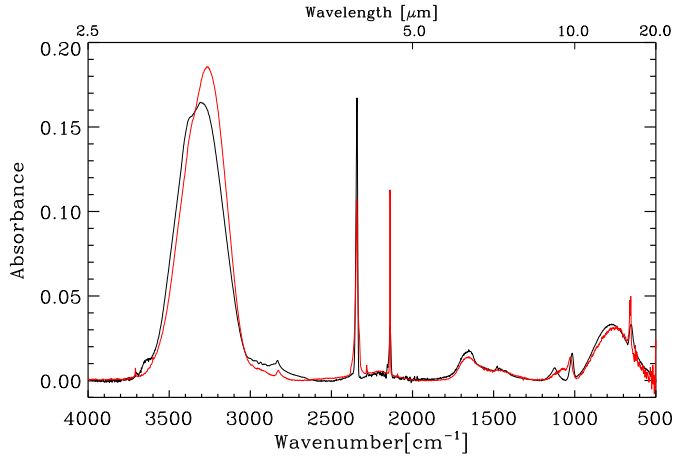

Figure 2: Black: IR spectrum of a pre-cometary ice mixture registered at 8 K. Red: Sum of the IR spectra of individual pure ice components registered at 8 K; they were multiplied by a factor to reproduce the composition of the pre-cometary ice mixture. (Martín-Doménech et al. 2014; reproduced with permission from Astronomy & Astrophysics, ©ESO)

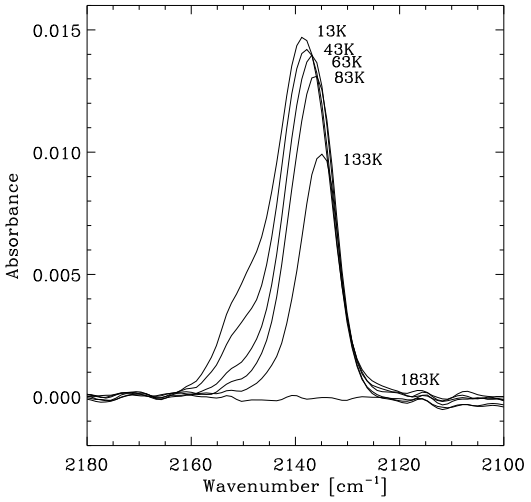

Figure 3: Evolution of the C=O stretching band of CO during the warm-up of a pre-cometary ice mixture. (Martín-Doménech et al. 2014; reproduced with permission from Astronomy & Astrophysics, ©ESO)

Figure 3 shows the gradual disappearance of the shoulder in the blue side of the C=O stretching band of CO during the warm-up, along with a redshift of the main peak. Therefore, no strong evidence of CO segregation is found in the IR spectra.

The evolution of the CO_2 stretching and bending bands is shown in the left and right panel of Fig. 4, respectively. The C=O stretching band at 2342 cm^{-1} is slightly redshifted at 8 K compared to its position in a pure CO_2 ice, and the redshift increases to 2339 cm^{-1} at higher temperatures. Moreover, the double peak structure of the degenerate bending modes does not appear. Again, there is no strong evidence of CO_2 segregation in our IR spectra.

Figure 5 shows the evolution of the umbrella mode of NH_3 at 1124 cm^{-1} and the C-O stretching mode of CH_3OH at 1016 cm^{-1}. The latter changes its band profile and peak frequency during the warm-up. Above a temperature of T $\sim$ 110 K before the onset of the desorption of CH_3OH, the peak shifts toward shorter wavelengths. At T $\sim$ 145 K, the band is broader and peaks at a frequency close to that of pure CH_3OH ice. At higher temperatures, the red component of the band gradually disappears and the peak is shifted to $\sim$ 1034 cm^{-1}. This indicates that a fraction of the CH_3OH molecules segregates in the ice at temperatures above T $\sim$ 110 K, while other CH_3OH molecules form a type II clathrate hydrate (Blake et al. 1991). Segregated molecules are able to desorb more easily than molecules in the clathrate hydrates, which mainly desorb at higher temperatures.

Since ice diffusion barriers are proportional to the volatility of the species (Öberg et al. 2009), the most volatile ones, like CO, can diffuse easily within the water ice structure. However, since the CO - CO interaction is the weakest among the species studied here, only small groups of segregated CO molecules can be formed before they reach the ice surface and desorb or, alternatively, the segregated-CO seed is torn apart by stronger interactions with other species. On the other hand, less volatile species like CH_3OH form hydrogen bonds with a similar strength to those formed by H_2O molecules (Bakkas et al. 1993), and desorb at higher temperatures compared to CO, CO_2, and NH_3. Therefore, segregated-CH_3OH seeds can grow without desorbing or being disrupted, forming larger regions

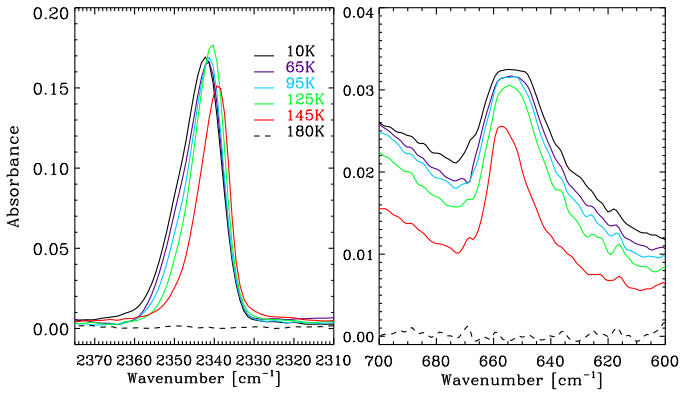

Figure 4: Evolution of the IR bands of CO_2 during the warm-up of a pre-cometary ice mixture. Left: C=O stretching mode at $\sim$ 2342 cm^{-1}. Right: bending mode at $\sim$ 655 cm^{-1}. (Martín-Doménech et al. 2014; reproduced with permission from Astronomy & Astrophysics, ©ESO)

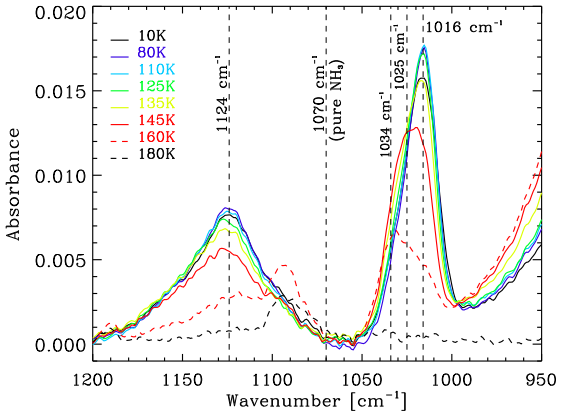

Figure 5: Evolution of the umbrella mode of NH_3 and the C-O stretching mode of CH_3OH during the warm-up of a pre-cometary ice mixture. (Martín-Doménech et al. 2014; reproduced with permission from Astronomy & Astrophysics, ©ESO)

which can be detected by the FTIR spectrometer.

4 Astrophysical implications

The heating rate used in our experiments is fast compared to most astrophysical scenarios, as it is generally the case in experimental simulations of astrophysical processes. The desorption behavior of an ice mixture does not strongly depend on the heating rate, but differences in the desorption temperatures are usually found (e.g., Collings et al. 2004). Using the kinetic parameters for pure H_2O ice desorption, Collings et al. (2004) performed a series of theoretical simulations of water ice desorption with different heating rates. The desorption peak reaches its maximum at T $\sim$ 160 K for a heating rate of 4.8 K/min, similar to the value used in our experiments and at T $\sim$ 105 K for a heating rate of 1 K/century, close to the heating rate in hot cores.

4.1 Circumstellar ices

The TPD curves and IR spectral evolution of our pre-cometary ice analogs allowed us to build a schematic representation of the thermal annealing process of ice mantles in circumstellar regions (Fig. 6). The heating rate applied to the pre-cometary ice mixtures in our experiments is of the same order of magnitude than that applied to ice mantles during the "flash-heating", as explained by the fluctuating X-wind model for CAIs and chondrules formation. Therefore, similar desorption temperatures are expected in this case. We have scaled laboratory temperatures to the scenario in which grains at a certain distance are heated as the temperature of the central object increases by multiplying them by a factor of 0.62. This factor corresponds to the ratio between the desorption peak temperature of water ice in our experiments ($\sim$ 170 K) and the one expected for a slower heating rate (1 K/century; Collings et al. 2004).

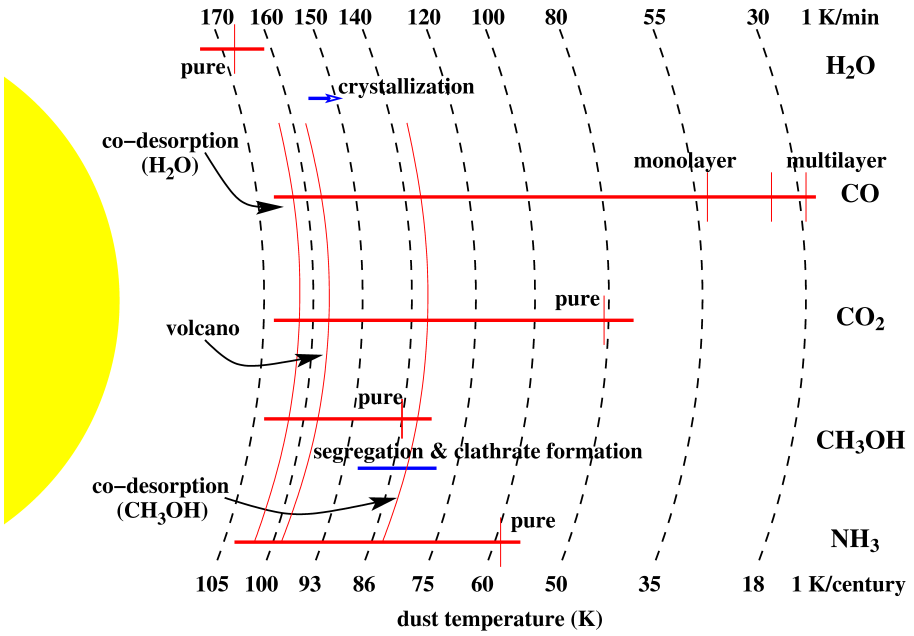

Figure 6: Schematic representation of thermal processing of ice mantles in circumstellar regions. Red lines and blue lines represent the temperature ranges at which the species used in our pre-cometary ice analogs desorb or structural changes in the ice occur, respectively. The top temperature scale corresponds to a heating rate of 1-2 K/min. The bottom temperature scale corresponds to a first approximation to grains at a certain distance heated with a heating rate of 1 K/century, see text for details. (Martín-Doménech et al. 2014; reproduced with permission from Astronomy & Astrophysics, ©ESO)

4.2 The ESA-Rosetta cometary mission

We expect to use the experimental data reported here as a benchmark for the analysis of the data collected by the mass spectrometers on board Rosetta as comet 67P/Churyumov-Gerasimenko is heated during its approach to the Sun.

Acknowledgements

We are grateful to Gustavo A. Cruz Díaz, Barbara Michela Giuliano, and Antonio Jiménez Escobar for their support on the experiments. This research was financed by the Spanish MINECO under projects AYA2011-29375 and CONSOLIDER grant CSD2009-00038. R. M. D. benefited from a FPI grant from Spanish MINECO.

References

Allamandola, L.J., Bernstein, M.P., Sandford, S.A., Walker, & R.L. 1999, Space Science Rev., 90, 219
Bar-Nun, A., Herman, G., & Laufer, D. 1985, Icarus, 63, 317
Bakkas, N., Bouteiller, Y., Louteiller, A., Perchard, J.P., & Racine, S. 1993, J. Chem. Phys., 99, 3335
Bisschop, S.E., Fraser, H.J., Öberg, K.I., van Dishoeck, E.F., & Schlemmer, S. 2006, A&A, 449, 1297
Blake, D., Allamandola, L., Sandford, S., Hudgins, D., & Freund, F. 1991, Science, 254, 548
Brown, W.A., Viti., S., Wolff, A.J., & Bolina, A.S. 2006, Faraday Discussions, 133, 113
Collings, M.P., Anderson, M.A., Chen, R., et al. 2004, MNRAS, 354, 1133
Fayolle, E.C., Öberg, K.I., Cuppen, H.M., Visser, R., & Linnartz, H. 2011, ApJ, 529, A74
Herbst, E. & van Dischoeck, E.F. 2009, Annu. Rev. Astron. Astrophys., 47, 427

Martín Doménech, R., Muñoz Caro, G.M., Bueno, J., & Goesmann, F. 2014, A&A, 564, A8
Mumma, M.J. & Charnley, S.B. 2011, Annu. Rev. Astron. Astrophys., 49, 471
Muñoz Caro, G.M., Jiménez-Escobar, A., Martín-Gago, J.A., et al. 2010, A&A, 522, A108
Öberg, K.I., Fayolle, E. C., Cuppen, H.C., van Dishoeck, E.F., Linnartz, H. 2009, A&A, 505, 183
Pauls, T.A., Wilson, T.L., Bieging, J.H., & Martin, R.N. 1983, A&A, 124, 123
Shu, F.H., Shang, H., & Lee, T. 1996, Science, 271, 1545
Shu, F.H., Shang, H., Glassgold, A.E., & Lee, T. 1997, Science, 277, 1475
Shu, F.H., Shang, H., Gounelle, M., Glassgold, A.E., & Lee, T. 2001, ApJ, 548, 1029
Smith, R.S., Huang, C., Wong, E.K.L., & Kay B.D. 1997, Phys. Rev. Lett., 79, 909
Viti, S. & Williams, D.A. 1999, MNRAS, 310, 517